

Contents lists available at ScienceDirect

Microporous and Mesoporous Materials

journal homepage: http://www.elsevier.com/locate/micromeso





Dual-template directed aminothermal syntheses and characterization of silicoaluminophosphates SAPO-CLO and ECR-40

Lijing Sun^{a,b}, Wenna Zhang^a, Zhuocheng Li^{a,b}, Miao Yang^{a,***}, Ye Wang^{a,c}, Xiaosi Zhang^{a,b}, Peng Tian^{a,**}, Zhongmin Liu^{a,b,*}

- a National Engineering Laboratory for Methanol to Olefins, Dalian Institute of Chemical Physics, Chinese Academy of Sciences, Dalian, 116023, Liaoning, China
- ^b University of Chinese Academy of Sciences, Beijing, 100049, China
- ^c College of Chemistry and Molecular Engineering, Zhengzhou University, Zhengzhou, 450002, Henan, China

ARTICLE INFO

Keywords: Aminothermal synthesis Dual-template SAPO-CLO ECR-40 Fluoride mineral agent

ABSTRACT

Two SAPO molecular sieves with -CLO and MEI topologies, named as SAPO-CLO and ECR-40F, were synthesized in an aminothermal environment with N,N-diethyl ethanolamine (DEEA) as both a solvent and an organic structure-directing agent (OSDA), and N,N,N-trimethylbutylammonium chloride (BTMACl) as a co-OSDA. The introduction of Si atoms into the aluminophosphate framework of DNL-1 has been evidenced by ²⁹Si MAS NMR. SAPO-CLO herein is the first SAPO material of -CLO topology with 20-ring channels, which is a metastable phase and could further convert to ECR-40F when the crystallization time is prolonged from 12 h to 48 h. The crystallization efficiency and solid yield of ECR-40F is dramatically improved compared with the previously reported synthesis of ECR-40. DEEA and BTMACl are new OSDAs for both materials. The location and role of the two templates have been well investigated through various comparative experiments, characterizations and simulated calculations. The strong alkaline aminothermal environment combining with the dual OSDAs and fluoride mineralizing agent promotes the crystallization of the two SAPO phases.

1. Introduction

Silicoaluminophosphate (SAPO) molecular sieves, as one class of the most important inorganic crystalline materials, have attracted extensive attentions from both industrial and academic fields due to their uniform microporous structures, large surface area, tunable acidity and high thermal/hydrothermal stabilities [1]. In particular, they are excellent heterogeneous solid acid catalysts with mild acidity and regular channel systems [2]. For example, the three-dimensional (3D) 8-ring openings and nanosized CHA cages of SAPO-34 enable 100% methanol conversion and more than 80% light olefins selectivity in the methanol conversion reaction [3]. In addition, the straight 1D 10- and 12-ring channels of SAPO-11 and SAPO-31 provide advantages for hydroisomerization of long-chain alkanes [4,5]. Considerable efforts have been made to explore new SAPO molecular sieves encouraged by their huge application potentials. Up to now, the number of identified SAPO molecular sieves is 40 in comparison to 44 for AlPO and 51 for MeAPO

molecular sieves [6]. The structure types of AlPO and SAPO molecular sieves are not equivalent although the formation of SAPO molecular sieves is generally regarded as isomorphous substitution of framework T atoms by Si. Some SAPO molecular sieves, such as SAPO-37 (FAU), SAPO-42 (LTA) and SAPO-56 (AFX), have no corresponding AlPOs but only aluminosilicate isostructural compounds [7]. Also, it is difficult for certain AlPO molecular sieves to complete the Si substitutions like AlPO-22 (AWW), STA-15 (SAF) and PST-13 (POR) [8–10]. The crystallization mechanism of molecular sieve materials is still an open issue. However, it is believed that the crystallization of molecular sieve materials strongly depends on many factors including the initial gel composition, temperature, crystallization time and so on.

Organic structure-directing agents (OSDAs) is a key factor whose geometry and charge density affect the product topology through filling the space and balancing the negative charges of the frameworks [11]. Corma and co-workers designed and selected a series of special OSDAs including quaternary ammonium cations, proton sponges, phosphonium

E-mail addresses: yangmiao@dicp.ac.cn (M. Yang), tianpeng@dicp.ac.cn (P. Tian), liuzm@dicp.ac.cn (Z. Liu).

https://doi.org/10.1016/j.micromeso.2021.110915

^{*} Corresponding author. National Engineering Laboratory for Methanol to Olefins, Dalian Institute of Chemical Physics, Chinese Academy of Sciences, Dalian, 116023, Liaoning, China.

^{**} Corresponding author.

^{***} Corresponding author.

cations and super basic phosphazenes to synthesize zeolites [12,13]. An extra-large-pore SAPO molecular sieve ITQ-51 with IFO topology has been achieved with large size proton sponges with high basicity and rigidity [14]. Co-templating strategy is another effective method to direct molecular sieves possessing different cage structures and channels. The combination of OSDAs allows the most appropriate OSDA to stabilize each structural part to achieve the most favorable interaction energy. Based on some successful examples of co-template synthesis [15–17], Wright et al. developed a retrosynthetic method to design the synthesis of target SAPO materials. SAPO-56 (AFX), STA-18 (SFW), STA-19 (GME) and STA-20 belonging to ABC-6 family with at least one *gme* cage per unit cell have been synthesized [18,19].

Besides OSDAs, solvent also has a strong influence on the crystalline products. The polarity, solubility, vapor pressure and other characteristics of solvent can change the status of reactants and crystallization mechanism resulting in different crystalline phase [20]. By using alcohol as a solvent with less polarity, a 20-ring AlPO compound JDF-20 can be crystallized with triethylamine (TEA) as a template [21]. In contrast, TEA directs 12-ring AlPO-5 in the corresponding hydrothermal condition. Ionic liquid became another popular solvent to synthesize microporous materials following the pioneer work of Morris et al. [22]. In particular, Tian et al. synthesized cloverite AlPO molecular sieve DNL-1 by using a co-templating ionothermal method in fluoride medium [23]. Ionic liquid 1-ethyl-3-methylimidazolate bromide ([Emim]Br) and another co-template 1,6-hexanediamine, tetrapropylammonium hydroxide or ammonium hydroxide have a cooperative nonbonded interaction which initiate the crystallization of DNL-1 [24]. The high thermal stability together with unique parallel and independent 8-ring and 20-ring channels system of DNL-1 makes it attractive in shape-selective sorption and catalytic process involved large molecules. Before DNL-1, the cloverite family has only (metallo)gallophosphate [25] and silicogermanate [26] compounds with poor stability which were synthesized in a hydrothermal fluoride medium. Until now, the synthesis of SAPO-type cloverite compound is still challenging [27]. In recent years, our group synthesized SAPO molecular sieves by using organic amines as solvents and OSDAs simultaneously. A lot of SAPO molecular sieves were synthesized efficiently, and some new OSDAs for directing SAPO-34 molecular sieve were found which may have significant effects on its acidity and MTO catalytic performance [28-30]. The intense interactions between the organic amines and inorganic species as well as the strong basic environment of aminothermal condition promote the crystallization of SAPO molecular sieves. Meanwhile, the crystallization pathway may change due to the shortage of water [31]. It is reasonable to expect some new SAPO phase under such an aminothermal system.

In this work, we report the synthesis of SAPO molecular sieves by using alkanolamine as both a solvent and template, with the assistance of quaternary ammonium salt co-template and fluoride mineralizing agent. Alkanolamine, possessing dual features of organic amine and alcohol, brings new opportunities for the discovery of SAPO molecular sieves. Two SAPO phases with –CLO (SAPO-CLO) and MEI (ECR-40F) topologies were synthesized. The introduction of Si atoms into CLO-AlPO framework has been confirmed by solid-state ²⁹Si MAS NMR. Meanwhile, there is an obvious improvement in the crystallization efficiency of ECR-40 (MEI) compared with the previous hydrothermal synthesis [32]. The phase selectivity between the two materials was found to be strongly dependent on kinetic factors. The framework of -CLO gradually converted to ECR-40F phase following the increase of crystallization time.

2. Experiment methods

2.1. Raw materials

The raw materials used include phosphoric acid (H₃PO₄, 85 wt%), silica sol (SiO₂, 31 wt%), pseudoboehmite (Al₂O₃, 77 wt%), N,N-diethyl ethanolamine (DEEA, 99 wt%), N,N,N-trimethylbutylammonium

chloride (BTMACl, 99 wt%) and hydrofluoric acid (HF, 40 wt%). All the chemicals were obtained from commercial suppliers and used directly without further purification.

2.2. Sample preparation

The aminothermal synthesis was similar to that of hydrothermal procedure. Typically, certain amounts of pseudoboehmite and silica sol were dissolved in DEEA solution one by one. After a thorough stir, phosphoric acid and BTMACl were added into the mixture followed by the addition of HF. The stirring was continuous during the addition of reactants. The mixture was rapidly sealed in a Teflon-lined stainless steel autoclave and heated to 200 $^{\circ}\text{C}$ for 12–48 h under rotation. The products were collected by filtration, washed with deionized water, and dried at 100 $^{\circ}\text{C}$ overnight. The samples were calcined at 600 $^{\circ}\text{C}$ for 3 h to remove the templates if necessary.

2.3. Characterization

The chemical compositions of the samples were obtained with a Philips Magix-601 X-ray fluorescence (XRF) spectrometer. The powder X-ray diffraction (XRD) patterns were recorded on a X'Pert PRO X-ray diffractometer with Cu-Ka radiation ($\lambda = 1.541 \text{ Å}$), operating at 40 KV and 40 mA. The crystal morphology of the samples was observed by scanning electron microscopy (SEM) on a Hitachi SU8020 field emission scanning electron microscopy. The textural properties of the calcined samples were tested by N2 adsorption at 77 K on a Micromeritics ASAP 2020 system. The total surface area was calculated based on the Brunauer-Emmett-Teller (BET) equation. The micropore volume and micropore surface area were evaluated using the t-plot method. Before analyses, the samples were calcined at 600 °C for 3 h in air, and then degassed at 350 °C for 4 h under vacuum. Thermogravimetric analysis was performed using a TA SDTQ600 analyzer which was heated from room temperature to 1200 °C with a heating rate of 10 °C min $^{-1}$ in an air flow of 100 mL/min.

Solid-state MAS 13 C, 29 Si, 27 Al and 31 P NMR were measured on a Bruker Avance III 600 spectrometer operated at a 14.1 T wide-bore magnet. The resonance frequency were 100.5, 119.2, 156.4 and 242.9 MHz for ¹³C, ²⁹Si, ²⁷Al and ³¹P MAS NMR, respectively. The spinning rates of the samples at the magic angle for ¹³C, ²⁹Si, ²⁷Al and ³¹P were 8, 10, 12 and 12 KHz, respectively. The reference materials for the chemical shift (in ppm) determination for ¹³C, ²⁹Si, ²⁷Al and ³¹P were 2,2-dimethyl-2-ilapentane-5-sulfonate sodium salt (DSS), (NH₄)Al $(SO_4)_2 \cdot 12H_2O$ and 85% H_3PO_4 respectively. ¹⁹F MAS NMR spectra were recorded on a 4 mm MAS probe using a spin echo pulse program with a spinning rate of 13 kHz. 16 scans were accumulated with a $\pi/2$ pulse width of 2.5 µs and a 5 s recycle delay. Chemical shifts were referenced to Na_3AlF_6 at -191 ppm. The ^{13}C liquid CP NMR spectra were performed on a Bruker Avance III 400 spectrometer equipped with a 9.4 T narrow-bore magnet, and the resonance frequency was 150.9 MHz. The deuterium solvent was D2O, and the chemical shifts were referenced to tetramethylsilane (TMS) at 0 ppm.

2.4. Calculation method of interaction energies

As a unit cell of DNL-1 contains more than 4000 atoms [7], a 74 T cluster model (Al $_{37}$ P $_{37}$ O $_{117}$) including α cage and rpa cage, extracted from the crystallographic data of -CLO structure, as shown in Fig. S1, represents the structure of SAPO-CLO zeolite for the theoretical calculations. The terminal Si–O bond was treated by hydrogen atoms saturating. During the structure optimizations, the combined theoretical ONIOM method including ω B97XD hybrid density function with 6-31G (d,p) basis sets and semi-empirical AM1 were employed for optimizing geometries of the high-level and low-level layer. All the atoms except for the terminal H atoms set as high layer. To obtain high accurate energies, the single-point energies were calculated at the level of ω B97XD/6-31G

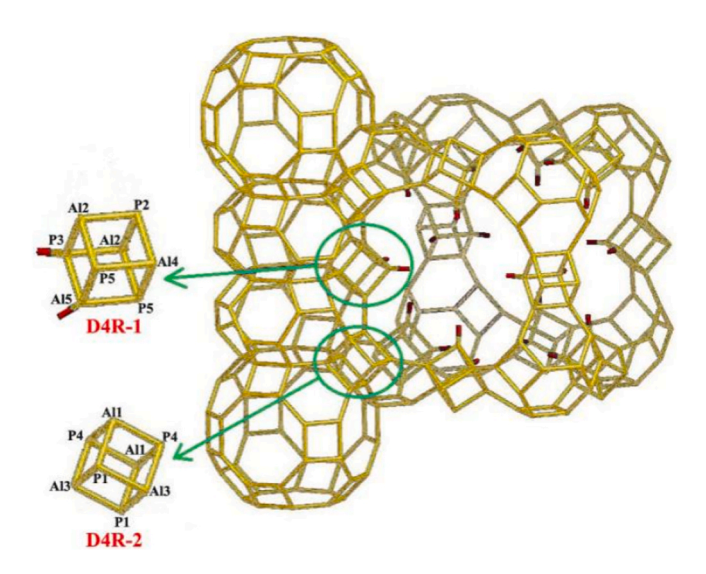


Fig. 1. Framework structure of DNL-1.

(d,p).

The interaction energy E_{inter} was calculated as: $E_{inter} = E - E_{zeolite} - E_{tem-plate}$, where E, $E_{zeolite}$, $E_{template}$ refer to calculation energies of the system of the template inside SAPO-CLO, SAPO-CLO framework and the template molecule, respectively. All density functional theory (DFT) calculations were performed with the Gaussian 09 package.

3. Results and discussion

Alkanolamines with both hydroxyl and amino groups possess strong basicity, polarity and miscibility with water, which are good solvents and templates for molecular sieve synthesis. Diglycolamine, diisopropanolamineand *N*-methyldiethanolamine etc. have ever been employed in the aminothermal synthesis of SAPO molecular sieves [8,29]. Herein, we explore the synthesis of SAPO molecular sieves in a dual-template aminothermal system. A mixed SAPO phase is first synthesized in DEEA aminothermal system with the assistance of BTMACl and HF at 200 °C for 24 h. After careful optimization of the crystallization condition, two pure SAPO-type crystalline phases with –CLO and MEI structures are achieved after crystallization of 12 h and 48 h, respectively.

3.1. Synthesis and characterization of SAPO-CLO

–CLO topology is an interrupted structure with extra-large 20-ring micropores. The structure consists of two types of double four rings (D4R) as the basic structural units, as shown in Fig. 1. The D4R-1 cages contain three inequivalent P atoms (P(2), P(3) and P(5)) and three inequivalent Al atoms (Al(2), Al(4) and Al(5)). The D4R-2 cages contain two inequivalent P atoms (P(1) and P(4)) and two inequivalent Al atoms (Al(1) and Al(3)). All the D4Rs link each other by sharing common corners creating α cages, rpa cages and 3D 8-ring and 20-ring channels along [100] direction. The 8-ring channels with a diameter of 3.8 Å run through the α and rpa cages, while the 20-ring channels are surrounded by the α and rpa cages, and form the supercage with a diagonal body of about 30 Å at the intersections. Four terminal hydroxyl groups (Al(5)-OH or P(3)-OH) extend from the D4R-1 units in each 20-ring windows [33].

DNL-1 was previously synthesized in an aluminophosphate ionothermal system, with no report on the synthesis of SAPO-type -CLO [23]. Thus, the crystallization of SAPO-CLO herein was well studied and the synthetic details are shown in Table 1. Without the addition of Si source, aluminophosphate DNL-1 crystallizes efficiently (sample D1) with a high yield of 83.9%. When the SiO_2/Al_2O_3 ratio is 0.3–0.5, SAPO-CLO crystallizes with a constant Si content of ca. 1% with a little

 Table 1

 The influence of gel composition on the synthetic results.

Samples ^a	R1:R2: Al ₂ O ₃ : P ₂ O ₅ :SiO ₂ : HF:H ₂ O ^b	Products	Product Compositions (molar ratio) ^c			Solid yields ^d
			Si/(Si + P + Al) (%)	F/ Al	Cl/ Al	(%)
D1	8.0: 1.0: 1.0: 1.0:	DNL-1	0	0.14	0.04	83.9
D2	0.0: 1.0: 15 8.0: 1.0: 1.0: 1.0:	SAPO-CLO	1.0	0.16	0.07	68.7
D3	0.3: 1.0: 15 8.0: 1.0: 1.0: 1.0:	SAPO-CLO	1.2	0.13	0.04	58.3
D4	0.5: 1.0: 15 8.0: 1.0: 1.0: 1.0:	amorphous	-	-	-	-
D5	0.7: 1.0: 15 8.0: 0.5: 1.0: 1.0:	SAPO-34& minor SAPO-	-	-	-	-
D6	0.5: 1.0: 15 8.0: 0.0: 1.0: 1.0:	42 SAPO-5& minor SAPO-	-	-	-	-
D7	0.5: 1.0: 15 4.0: 1.0: 1.0: 1.0:	34 SAPO-CLO	1.4	0.13	0.00	66.2
D8	0.5: 1.0: 15 2.0: 1.0: 1.0: 1.0:	SAPO-CLO	1.1	0.15	0.06	70.8
D9	0.5: 1.0: 15 1.0: 1.0: 1.0: 1.0:	DNL-1 & impurity	-	-	-	
D10	0.5: 1.0: 15 8.0: 1.0: 1.0: 1.0:	DNL-1	0.4	0.33	0.00	28.7
D11	0.5: 2.0: 15 8.0: 1.0: 1.0: 1.0:	amorphous	6.8	0.08	-	-
D12	0.5: 0.5: 15 8.0: 1.0: 1.0: 1.0:	amorphous	-	-	-	-
D13	0.5: 0: 15 8.0: 1.0: 1.0: 1.0:	SAPO-CLO	4.3	0.18	0.15	84.3
D14	0.5: 1.0: 10 8.0: 1.0: 1.0: 1.0: 0.5: 1.0: 30	amorphous	-	-	-	-

 $^{^{\}rm a}$ All samples are crystallized at 200 $^{\circ}\text{C}$ for 12 h under rotation.

decreased solid yield. Continuously increased Si dosage causes amorphous phase. The results show the difficulty of Si doping for DNL-1. The influences of various synthetic parameters are systematically investigated. The reduction or absence of BTMACl leads to SAPO mixtures of SAPO-34 and SAPO-42 or SAPO-5. Considering that both SAPO-5 and SAPO-34 have no D4R subunits, it is believed that the presence of BTMACl is helpful for the formation of D4R structure. The dosage of DEEA can be adjusted in a wide range and pure SAPO-CLO is obtained within the DEEA/Al₂O₃ ratio of 2–8. But the required amount of HF and H₂O are quite critical. Increasing the HF/Al₂O₃ ratio to 2.0, which is a comparable amount of the reported ionothermal synthesis of DNL-1 [23], the Si content of product D10 decreases to ca. 0.4% and the F content is double that of D3. When the HF/Al₂O₃ ratio is reduced to 0.5-0 or the H₂O/Al₂O₃ ratio is increased to 30, the products are amorphous. On the contrary, reducing H2O/Al2O3 ratio to 10 (all the H₂O comes from the raw materials) can achieve SAPO-CLO with increased Si content of ca. 4.3% (sample D13) with a high yield of 84.3%. The purity and high crystallinity of D13 have been confirmed by

^b R1 and R2 are DEEA and BTMACl, respectively.

^c Determined by XRF.

^d Yield = $W_{product}*70\%/W_{SiO22+P2O5+Al2O3}$.

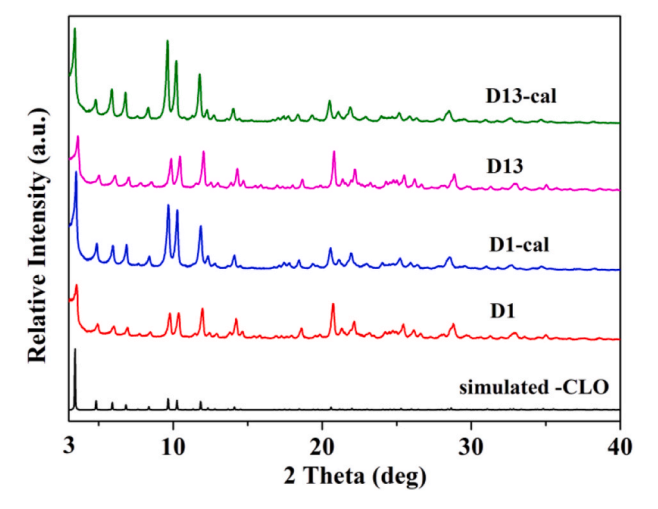


Fig. 2. XRD patterns of simulated, as-synthesized and calcined D1 and D13.

XRD, SEM and N_2 adsorption etc., whose details are given below. The results illustrate that both DEEA and BTMACl are necessary for the crystallization of SAPO-CLO. A more concentrated condition favors the incorporation of more Si atoms into the AlPO-CLO framework, whereas too much HF has negative effects on the formation of SAPO-CLO.

The XRD patterns of the as-synthesized and calcined D1 and D13 are shown in Fig. 2. All the diffraction peaks are identical to those of the simulated XRD patterns based on -CLO structure indicating their purity. After calcination, the peak intensity of calcined D1 and D13 is improved, showing their high thermal stability. The SEM images of D1 and D13 are shown in Fig. 3. The samples have typical cubic morphology with crystal size of 200–500 nm, and no amorphous particles can be found for both samples confirming their purity. Comparatively, the crystals of ionothermal synthesized DNL-1 are cubes with the size of 10–30 μm [34]. The textual properties of D1 and D13 were characterized by N_2 physical adsorption. Fig. 4a exhibits typical I plus IV type isotherms with H4 type hysteresis loops in the region 0.4 < P/P0 < 1.0, indicating the coexistence of micropores and mesopores. In particular, their micropore surface area (691 and 597 $m^2 g^{-1}$) and micropore volumes (0.32 and 0.29 $cm^3 g^{-1}$) are much larger than those of ionothermal synthesized ones (see

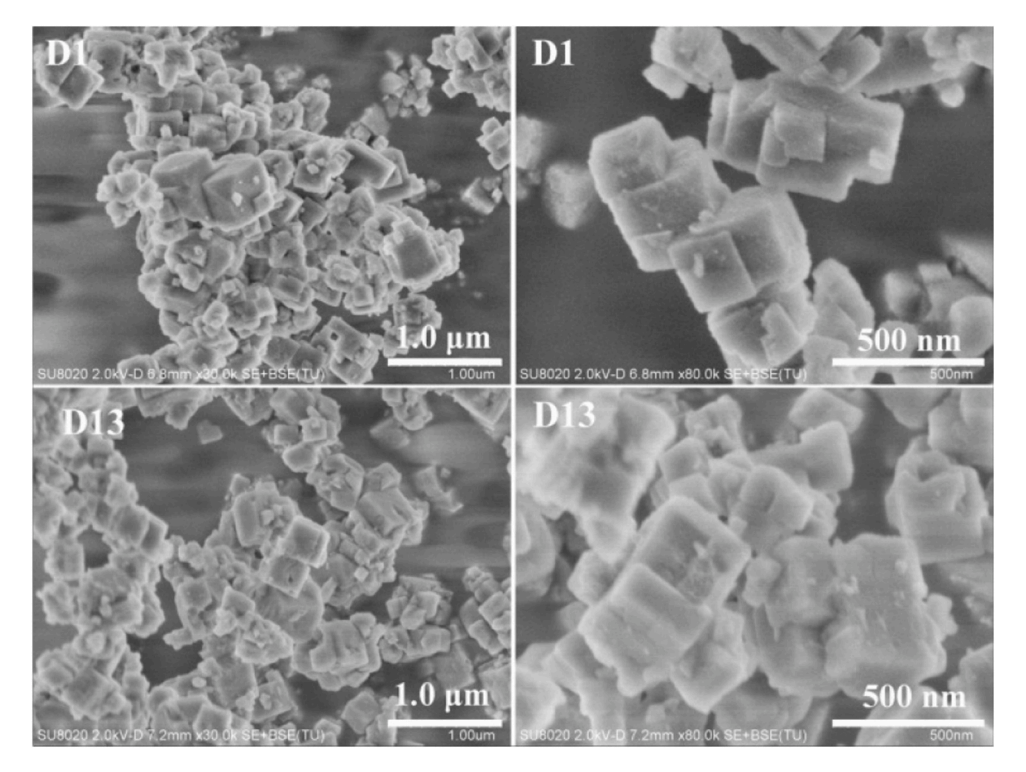


Fig. 3. SEM images of D1 and D13.

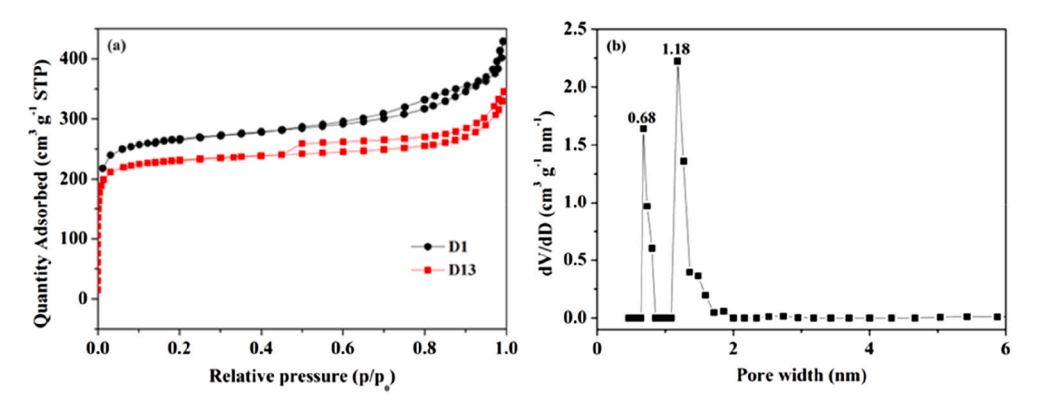


Fig. 4. (a) N₂ adsorption-desorption isotherms of D1 and D13 and (b) pore size distributions of D13 calculated by DFT method.

Table 2 Textural properties of D1 and D13.

Samples	Surface area (m ² g ⁻¹)		Pore volume (cm ³ g ⁻¹)		
	S _{total} ^a	S_{micro}^{b}	S _{ext} ^c	V _{total}	V_{micro}^{d}
D1	903	691	212	0.58	0.32
D13	746	597	149	0.47	0.29
DNL-1 [23]	631	485	146	0.42	0.20

- a BET surface area.
- ^b *t*-plot micropore surface area.
- $^{\rm c}$ *t*-plot external surface area.
- ^d *t*-plot micropore volume.

Table 2) [23], verifying the better crystallinity of SAPO-CLO. DFT pore size distribution curves (Fig. 4b) of D13 exhibits two peaks at 0.68 and 1.18 nm agreeing with the 8-ring and 20-ring channels of DNL-1.

Solid-state ²⁷Al, ³¹P, ¹⁹F and ²⁹Si MAS NMR spectra are recorded to investigate the atomic coordination environments of as-synthesized D1 and D13 (Fig. 5). The ²⁷Al, ³¹P and ¹⁹F MAS NMR spectra of D1 are similar to those of the reported DNL-1 but with subtle differences [33]. The ²⁷Al MAS NMR spectrum of D1 displays a strong resonance at 35.1 ppm with a shoulder resonance at 25.0 ppm and a small independent peak at –2.6 ppm. The peak at 35.1 ppm corresponds to tetrahedrally coordinated Al, and the other two signals are assigned to five coordinated Al connecting to one terminal F and octahedral Al coordinated with two guest molecules respectively [33,34]. The ²⁷Al MAS NMR peaks of D13 migrate to high field with a narrower shape. The shoulder resonance disappears suggesting the missing of terminal F. Another very small signal rises at –9.2 ppm due to six coordinated Al. The ³¹P MAS NMR spectrum of D1 exhibits three main signals at –30.3, –20.5 and –11.6 ppm. According to the reference, the peak at –30.3 ppm is

ascribed to P(2)O₄ and P(3)O₄groups, and the peak at -20.5 ppm assigned to P(1)O₄, P(4)O₄ and P(5)O₄ groups [33]. Additionally, the peak at -11.6 ppm is associated with P(3) connecting to terminal OH groups. Comparatively, the peak at -30.3 ppm is missing for D13. The substitution of P by Si atoms might reduce the crystallographic site of P. The ¹⁹F MAS NMR spectra reveal more characters of D1 and D13. Both D1 and D13 have two strong ¹⁹F signals at -95.2 and -97.4 ppm attributed to F⁻ anions trapped in D4R-1 and D4R-2 units [33]. Different from the reported result of DNL-1, the terminal F- anions signal at -101.9 ppm is much smaller for D1 and even missing for D13 [23,35]. This might be associated with the less HF dosage in aminothermal synthesis resulting in lower F content for products. More importantly, the ²⁹Si MAS NMR spectrum of D13 further confirms the introduction of Si atoms. It displays three resonances at -83.7, -91.4 and -100.5 ppm assigned to $Si(OAl)_nOH_{4-n}(n = 1,2)$, $Si(OAl)_4$ and $Si(OAl)_2(OSi)_2$, respectively. Combining the missing peak at -30.3 ppm in 31 P MAS NMR spectrum of D13, Si atoms probably substitute the sites of P(2) and P(3) in D4R-1 (Fig. 1). This substitution causes negative charges to the framework where the linkage of F⁻ anions seems to be not necessary any more. This agrees with the absence of MAS NMR signals of terminal F and five-coordinated Al.

Considering that SAPO-CLO has a lower F content (F/Al = 0.16) than that of the ionothermally synthesized DNL-1 (F/Al = 0.33), the successful synthesis of SAPO-type cloverite compound may thank to the concentrated aminothermal environment and suitable hydrofluoric acid dosage. Many AlPO molecular sieves such as AlPO EMM-8 and AlPO-34 are synthesized in a neutral or acidic environment with a fluoride media, while their corresponding SAPO molecular sieves are synthesized in alkaline environment with a low F level or none fluoride [35–37]. Xu et al. investigated the influence of F^- anions on D4R units by

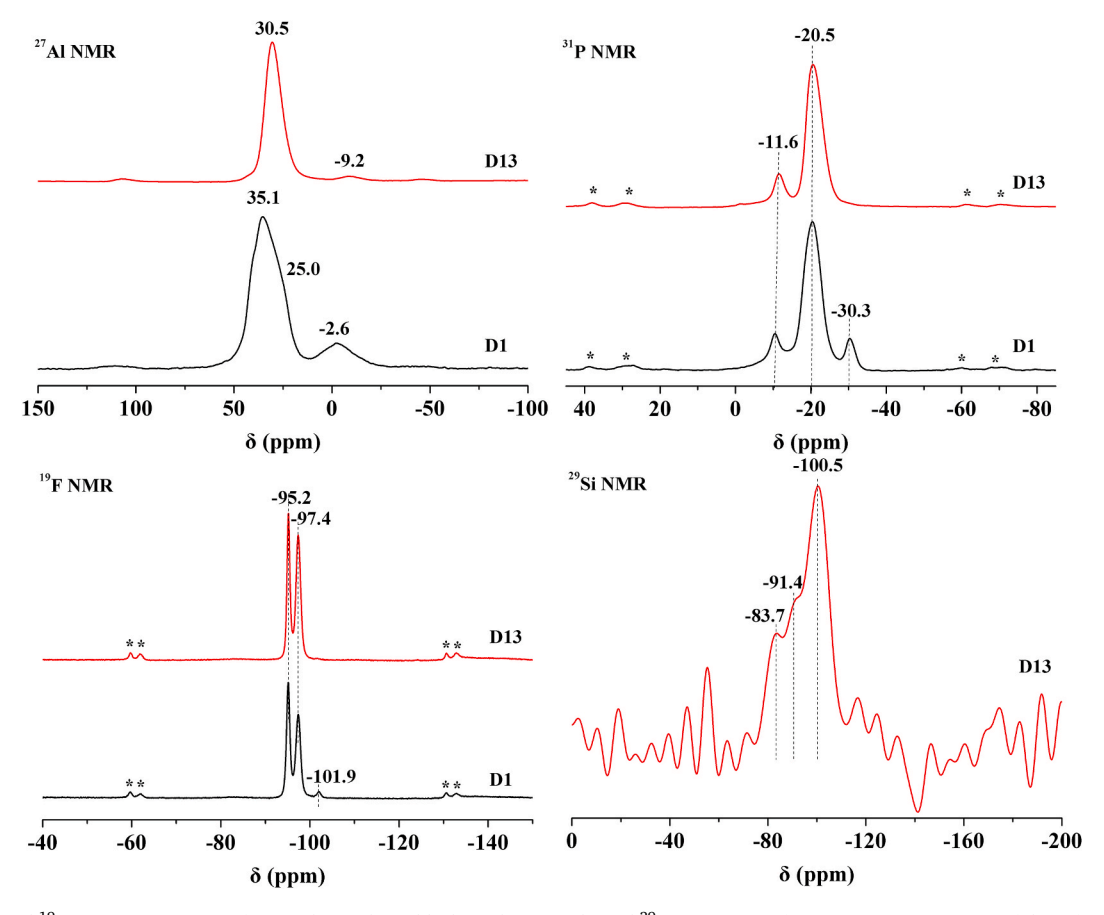


Fig. 5. ²⁷Al, ³¹P and ¹⁹F MAS NMR spectra of as-synthesized D1 (black) and D13 (red), and ²⁹Si MAS NMR of D13. (For interpretation of the references to colour in this figure legend, the reader is referred to the Web version of this article.)

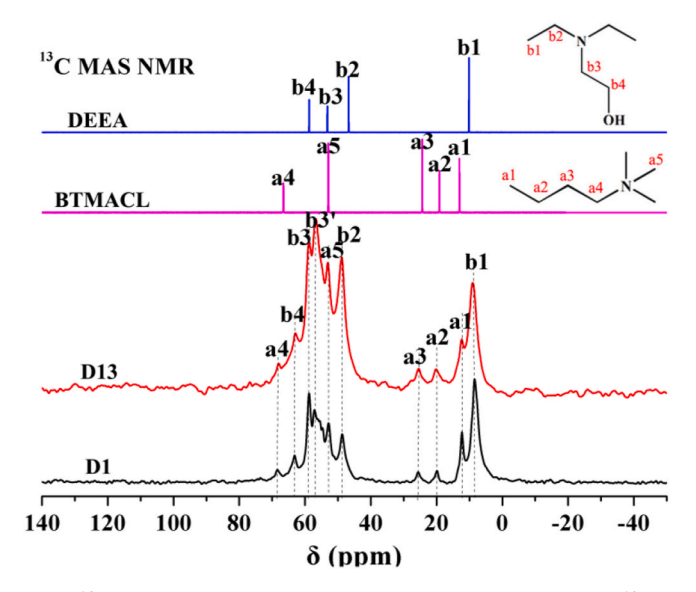


Fig. 6. 13 C CP NMR spectra of BTMACl and DEEA raw materials and 13 C CP MAS NMR spectra of D1 and D13.

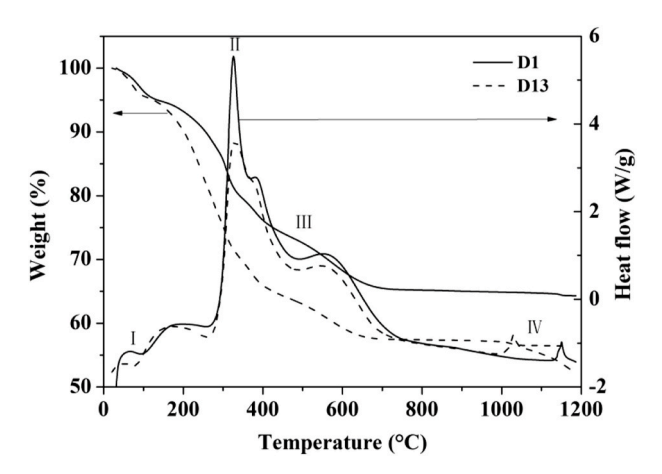


Fig. 7. TG/DSC curves of as-synthesized D1 and D13.

quantum-chemical calculation [38]. F^- anions enhance the stabilities of full P–Al D4R units, while obstruct the stability of Si–Al cluster. Thus, the presence of fluoride anions has a negative effect on the crystallization of SAPO materials with D4Rs. In the ionothermal synthesis of DNL-1, the neutral synthetic environment and high HF dosage may prevent Si atoms imbedding into the framework. In the current system, the concentrated aminothermal environment has a stronger alkalinity (pH = 10–11) which may accelerate the dissolution of Si source, and provide abundant OSDAs simultaneously for the crystallization of SAPO materials. Meanwhile, the half dosage of HF favors the formation of SAPO framework.

The status of dual templates was identified by comparison of the ¹³C CP NMR results. Although there are peak shifts between the results of ¹³C CP NMR spectra of raw material BTMACl and DEEA and solid-state ¹³C CP MAS NMR spectra of D1 and D13, as shown in Fig. 6, the coexistence of BTMACl and DEEA in the as-synthesized samples can be confirmed. The peaks at 12.1 (a1), 19.8 (a2), 25.6 (a3), 68.4 (a4) ppm can be ascribed to the carbon atoms in butyl (a1-a4) groups, and the peak of 56.8 (a5) ppm assigned to methyl (a5) groups of BTMACl correspondingly [39,40]. The peaks at 8.6 (b1) and 48.8 (b2) arose from the ethyl groups, while the ones at 56.6 (b3), 58.6 (b3') and 63.1 (b4) ppm ascribed to ethoxyl groups of DEEA [41,42]. The splitting of b3 peak implies that the occluded DEEA may adopt at least two

Table 3 Thermal analysis results of D1 and D13.

Samples	Weight loss (%)					
	I (<120 °C)	II (120–330 °C)	III (330–700 °C)	IV (D1: 1150 °C, D5: 1030 °C)		
D1 D13	5.0 4.9	14.2 22.9	16.0 15.4	0		

conformations [8].

The location and amounts of the two OSDAs were further investigated by TG/DSC analyses. The thermogravimetric behavior of D1 and D13 are shown in Fig. 7 and Table 3. The main discrepancy of the two samples lies in the weight loss from 120 to 330 °C. 14.2 wt% for D1 vs. 22.9 wt% for D13, which corresponds to the removal of OSDA in 20-ring channels. The weight losses from 330 to 700 °C for D1 and D13 are 16.0% and 15.4% respectively, corresponding to the elimination of organic molecules in the 8-ring channels together with the removal of F and hydroxyl groups [43]. In addition, there are two small exothermic peaks at 1150 and 1030 °C in DSC profiles of D1 and D13 without any corresponding weight loss. This thermal behavior is ascribed to the framework collapse indicating their high thermal stability. The TG/DSC results indicate the dual OSDAs stay in both 20-ring supercages and the 8-ring channels which consist of α and rpa cages. Since the similar size and molecular weight of DEEA and BTMACl, it is very difficult to identify their real locations by experimental characterization. Combined with the product compositions (Table 1), TG analysis and the framework charge balance rule, the possible formulas of D1 and D13 speculated $(C_6H_{15}NO)_{212}(C_7H_{18}ClN)_{32}(C_7H_{18}N)_1$ were as $_{06}\mathrm{H}_{2}\mathrm{O}_{374}(\mathrm{Al}_{768}\mathrm{P}_{768}\mathrm{O}_{2976}(\mathrm{OH})_{192}\mathrm{F}_{106})$ $(C_6H_{15}NO)_{275}(C_7H$ and $_{18}\text{ClN})_{107} (\text{C}_7 \text{H}_{18} \text{N})_{145} \text{H}_2 \text{O}_{389} (\text{Al}_{740} \text{P}_{730} \text{Si}_{66} \text{O}_{2976} (\text{OH})_{192} \text{F}_{135}) \quad \text{ respective properties of the control of$ tively. More BTMA+ cations are introduced in D13 to compensate the negative charges of SAPO-CLO framework. The interactions between OSDAs and various cavities (α cage and rpq cage) are further calculated to speculate the distribution of OSDAs. As a unit cell of DNL-1 contains more than 4000 atoms, it is hard to calculate the whole unit cell. And the big 30 Å supercage can be regarded as mesoporous where the templates can move freely. So a 74 T cluster model including α cage and rpa cage is extracted from the crystallographic data of -CLO structure for the theoretical calculations. The detailed interaction energies for the OSDAs in different cavities are given in Fig. 8. Obviously, when DEEA locates in the α cage and BTMACl displays in the *rpa* cage, the system exhibits high stability with highest interaction energy of -396.1 kJ/mol. This result indicates DEEA and BTMACl prefer to occupy α and rpa cages, respectively, showing the collaboration of DEEA and BTMACl on the formation of SAPO-CLO.

3.2. Synthesis and characterization of ECR-40

ECR-40, first reported by Strohmaier et al., in 2004 [32], is known as special inorganic-organic hybrid SAPO material odd-numbered-ring MEI structure and Al-O-Al bonds which violates the famous "löwenstein's rule". It has no aluminophosphate isomorphs but aluminosilicate analogues ZSM-18 [44] and UZM-22 [45]. The absence of aluminophosphate MEI structure should be because the connections of AlO₄ and PO₄ tetrahedra cannot form 3-ring units [32]. Alkanolamines are suitable OSDAs for ECR-40, whose hydroxyl groups may bond to framework Al atoms forming Al-OSDA complex and results in Al-O-Al linkages after the removal of OSDAs, as shown in Fig. 9a [42]. Five OSDAs have been reported to direct ECR-40A-E respectively in a hydrothermal environment. They are tris(2-hydroxyethyl) methylammonium (THMA⁺), bis(2-hydroxyethyl)dimethylammonium (BHDMA⁺), (2-hydroxyethyl)trimethylammonium (HTMA⁺), (2-hydroxyethyl)methylamine (BHMA) and bis(2-hydroxyethyl) ethylamine (BHEA) respectively, as shown in Fig. 9b. Except ECR-40A synthesized by THMA+, all the syntheses of ECR-40B-E needs the aid

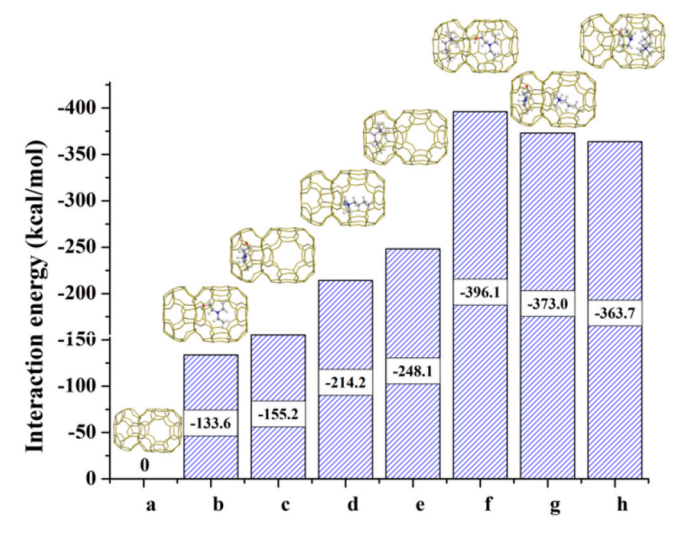


Fig. 8. The interaction energies of different situations: (a) empty rpa and α cage, (b) DEEA in α cage with empty rpa cage, (c) DEEA in rpa cage with empty rpa cage, (d) BTMACl in rpa cage with empty rpa cage, (e) BTMACl in rpa cage with empty rpa cage, (f) DEEA in α cage and BTMACl in rpa cage, (g) BTMACl in α cage, DEEA in rpa cage and (h) DEEA and BTMACl in the α cage with empty rpa cage. (-CLO framework: yellow, N atoms: blue, C atoms: grey, H atoms: white and O atoms: red). (For interpretation of the references to colour in this figure legend, the reader is referred to the Web version of this article.)

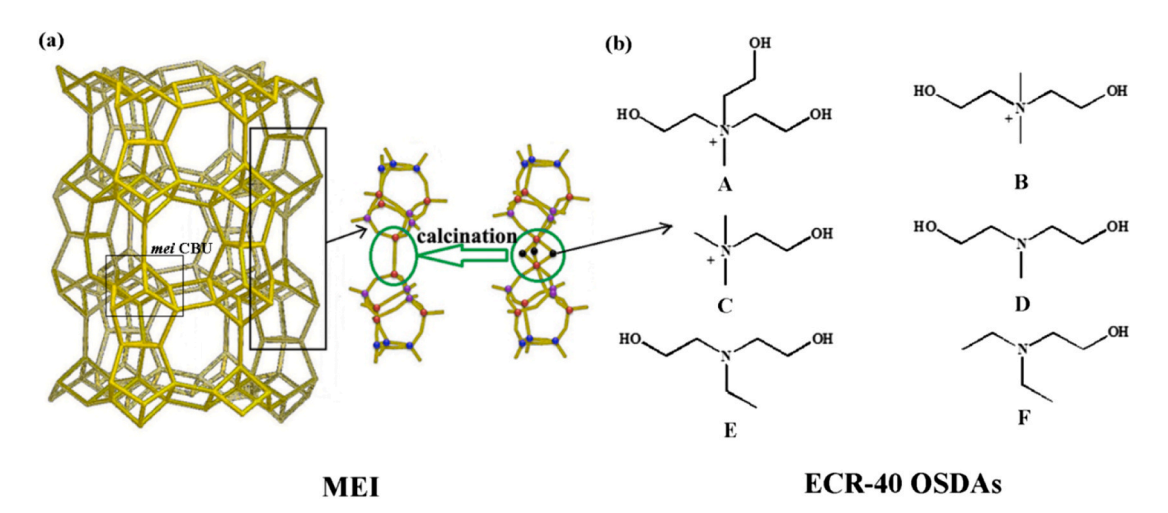


Fig. 9. (a) MEI topology and partial structure (Si: blue, Al: red, P: purple, OSDA: black dots). (b) Alkanolammonium ions and alkanolamines employed as OSDAs of ECR-40: A. THMA⁺, B. BHDMA⁺, C. HTMA⁺, D. BHMA, E. BHEA and F. DEEA (our work). (For interpretation of the references to colour in this figure legend, the reader is referred to the Web version of this article.)

of ECR-40 or UZM-22 seed. Moreover, it takes at least 12 days for their crystallization with very low yields (less than 14%) [32]. Herein, we report the efficient crystallization of ECR-40, denoted ECR-40F, by using DEEA as a template and a solvent in the presence of BTMACl and HF.

The synthetic details are shown in Table 4. DNL-1 was the final product when silica is absent. ECR-40F phase appears as the introduction of silica dosage. When the ${\rm SiO_2/Al_2O_3}$ ratio was in the range of 0.3–0.5, pure ECR-40F was achieved after crystallization at 200 °C for 48 h under rotation. SAPO-CLO can be seen as an intermediate phase during its crystallization, as shown in Table S1. When the crystallization time is prolonged to 24 h, the product is a mixture of ECR-40 and SAPO-CLO with a solid yield of 48%. Pure ECR-40 is achieved at 36 h with the Si content of 17.6 and a yield of 64.9%. Considering that the MEI topology has no D4R but *mei* composite building units (CBUs). It is believed that the D4R composed by AlPO₄ should be more stable than the Si inserted one. With the introduction of Si atoms, the D4R CBUs decompose which form *mei* type linkages. Impurity SAPO-34 appeared when silica source was further increased. The aminothermal and watershortage environment is also necessary for the crystallization of ECR-40.

A mixture of amorphous material and minor SAPO-34 (sample E7) was obtained when the synthesis was carried out under hydrothermal condition (pH ~9.0), even with prolonged crystallization time as the reported condition [32]. High concentration of alkanolamine leads to a stronger alkalinity (pH = 10–11) which may accelerate the dissolution and rebinding of the inorganic reactants. More locally ordered structural units generated by the dissolution of the SAPO-CLO conspicuously boost the crystallization of ECR-40. It is noted that the crystallization of ECR-40F cannot be realized without the addition of BTMACl as seen in the results of E8 and E9 in Table 4.

The XRD patterns of the as-synthesized and calcined E5 are shown in Fig. 10a. The peaks agree with the reported XRD pattern of ECR-40 without additional peaks [42]. The XRD peak positions of calcined E5 slightly migrate, and the peak intensity decreases obviously after calcination in air. Nevertheless, the in-situ temperature-programmed XRD patterns in N_2 atmosphere (Fig. S3) are kept well showing their high thermal stablility in N_2 . The framework of ECR-40 is sensitive to water as the Al-O-Al bond tends to decompose under the attacks by water [42]. The N_2 physical adsorption results (Fig. 10b) exhibit a high

Table 4The influence of gel composition^a on the synthetic results.

Samples	$X SiO_2$	Products	Product compositions b	Solid yields ^c (%)
E1	0	DNL-1	-	67.6
E2	0.1	SAPO-CLO & minor ECR-40	_	_
E3	0.2	ECR-40 & minor SAPO-CLO	_	_
E4	0.3	ECR-40	$Al_{0.447}P_{0.398}Si_{0.155}O_2$	66.2
E5	0.5	ECR-40	$Al_{0.459}P_{0.367}Si_{0.174}O_2$	65.0
E6	0.8	ECR-40 & minor SAPO-34	_	_
$E7^d$	0.5	amorphous& minor SAPO-34	_	_
$E8^e$	0.5	SAPO-5	_	_
E9 ^f	0.75	SAPO-5&SAPO-34	_	_

^a The molar ratio is 8.0 DEEA: 1.0 BTMACl: 1.0 Al₂O₃: 1.0 P₂O₅: X SiO₂: 1.0 HF: 15 H₂O, X = 0-0.8; the samples are crystallized at 200 °C for 48 h under rotation.

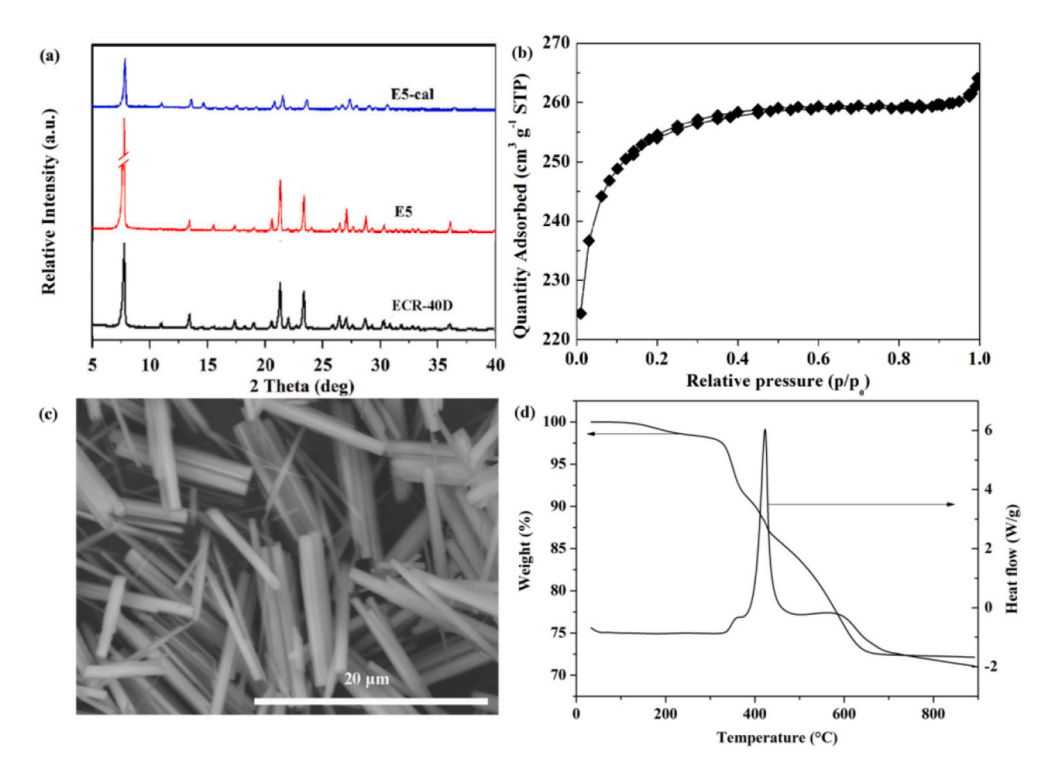


Fig. 10. (a) XRD patterns of reported ECR-40D [43], as-synthesized and calcined E5. (b) N_2 adsorption-desorption isotherm, (c) SEM image and (d) TG/DSC curves of E5.

micropore surface area of 733 $\rm m^2g^{-1}$ and micropore volume 0.34 $\rm cm^3g^{-1}$. The SEM image (Fig. 10c) reveals that ECR-40 crystals are long rod shaped with $\it ca.$ 40 depth-diameter aspect ratio. The thermal behavior of E5 was investigated by TG/DSC analysis (Fig. 10d). The sample has only $\it ca.$ 2.5 wt% weight loss before 300 °C followed by $\it ca.$ 25 wt% weight loss from 300 to 650 °C. The higher decomposition temperature of OSDAs should ascribe to the chemical bonding interaction between OSDA and the framework.

The chemical environments of sample E5 are investigated by solidstate 27 Al, 31 P and 29 Si MAS NMR (Fig. 11). The 27 Al MAS NMR spectrum displays three peaks at 41.9, 34.0 and -6.1 ppm. The peaks at 41.9 and 34.0 ppm are assigned to tetrahedrally coordinated Al at inequivalent positions and the peak at -6.1 ppm is assigned to six-coordinated Al bonded to OSDA [42]. The ³¹P spectrum presents a single resonance at -26.4 ppm assigned to the tetrahedrally coordinated P species. The ²⁹Si MAS NMR spectrum shows some overlapped peaks around 109.7 ppm. The peaks at -90.3, -94.9, -101.8, -105.6 and -109.7 ppm are assigned to Si(OAl)₄, Si(OAl)₃(OSi)₁, Si(OAl)₂(OSi)₂, Si (OAl)₁(OSi)₃ and Si-island, respectively [46]. Normally, the Si atoms prefer to locate at the 3-ring and form Si–O–Si structure in the ideal ECR-40 framework with Si(OAl)₂(OSi)₂ distribution [42]. The abundant Si(OAl)₁(OSi)₃ and Si-island species in E5 probably caused by the special aminothermal environment with fluoride media. The use of fluoride media tends to decrease the negative charge of open framework since F

b Determined by XRF.

^c Calculation based on the following equation: Yield = W_{product}* 70%/W_{SiO2+P2O5+Al2O3}.

 $^{^{\}rm d}$ The molar ratio is 2.0 DEEA: 1.0 Al₂O₃: 0.75 P₂O₅: 0.75 SiO₂: 80 H₂O, 160 $^{\circ}$ C for 120 h under rotation.

^e The molar ratio is similar to E5 but without BTMACl.

 $^{^{\}rm f}\,$ The molar ratio is similar to E5 but without BTMACl and HF.

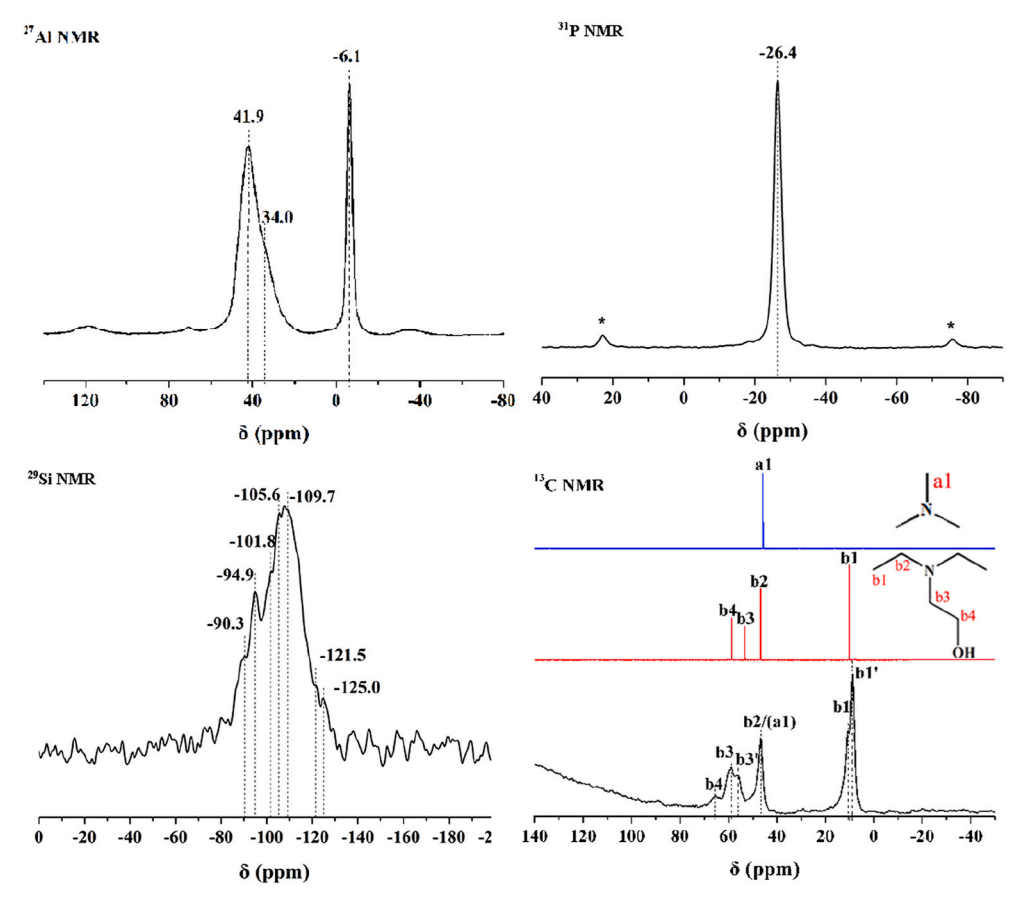


Fig. 11. Solid-state ²⁷Al, ³¹P, ²⁹Si and ¹³C MAS NMR spectra of E5 and ¹³C CP NMR spectra of DEEA and TMA raw material.

anions may balance the positive charges of protonated OSDA molecules [47]. As a result, too much F^- ions prohibits the introduction of Si atoms into almuminophosphate framework resulting in AlPO-CLO. The Si atoms can be introduced only when the amount of HF is reduced. However, the SAPO-CLO is unstable as the increased Si doping which decompose and convert to ECR-40. The formation of Si-islands is inevitable in order to reduce the framework charge and accommodate abundant Si atoms.

The ¹³C CP MAS NMR spectrum of E5 and ¹³C CP NMR spectra of OSDAs raw materials are shown in Fig. 11. The four group peaks at 8.7 (b1), 10.5 (b1'), 46.5 (b2), 55.9 (b3), 58.6 (b3') and 65.5 (b4) ppm can be assigned to the carbon of methyl and methylene in ethyl and ethanol groups of DEEA respectively. The shifts differences with those of SAPO-CLO are owing to the different environments of DEEA in the different chemical environment. The splitting of peaks b1and b3 implies more than one conformation for DEEA in E5 [8]. The characteristic resonance of BTMACl cannot be found in ¹³C CP MAS NMR spectrum. BTMACl may not remain in E5 or has been decomposed to trimethylamine (TMA) whose characteristic ¹³C NMR peak overlaps with peak b2 [48] although BTMACl has been confirmed to be necessary for the crystallization of ECR-40.

4. Conclusion

SAPO cloverite compound SAPO-CLO with high crystallinity has been synthesized by using DEEA as a solvent and template, and BTMACl as a cooperative template. The insertion of Si atoms into the –CLO aluminophospahte framework thanks to the cooporation of strong alkaline gel environment, dual templates and fluoride mineralizing agent. As evidenced by ²⁹Si MAS NMR, the main Si environments in SAPO-CLO are Si(OAl)₄ and Si(OAl)₂(OSi)₂. The formation of SAPO-CLO phase is

controlled actually by crystallization kinetics. ECR-40F as the sixth member of ECR-40 family crystallizes from the same reactant mixture as the prolonged reaction time. Compared to the previously hydrothermal synthesis, the crystallization time of ECR-40 is dramatically reduced to 48 h and the solid yield is greatly increased to 65%. These results encourage more explorations of SAPO materials in the aminothermal dual-template synthesis.

CRediT authorship contribution statement

Lijing Sun: Conceptualization, Methodology, Validation, Formal analysis, Investigation, Writing - original draft. Wenna Zhang: Formal analysis, Software. Zhuocheng Li: Investigation. Miao Yang: Methodology, Writing - review & editing, Funding acquisition. Ye Wang: Validation. Xiaosi Zhang: Validation. Peng Tian: Writing - review & editing, Supervision, Funding acquisition, Project administration. Zhongmin Liu: Supervision, Project administration.

Declaration of competing interest

The authors declare that they have no known competing financial interests or personal relationships that could have appeared to influence the work reported in this paper.

Acknowledgements

The authors thank the financial support of the National Natural Science Foundation of China (No. 21676262, 21991090, 21991091), the Key Research Program of Frontier Sciences, CAS (Grant No. QYZDB-SSW-JSC040) and the Innovation Research Foundation of Dalian Institute of Chemical Physics, Chinese Academy of Sciences (No.DICP

I201909).

Appendix A. Supplementary data

Supplementary data to this article can be found online at https://doi.org/10.1016/j.micromeso.2021.110915.

References

- [1] M. Moliner, C. Martinez, A. Corma, Synthesis strategies for preparing useful small pore zeolites and zeotypes for gas separations and catalysis, Chem. Mater. 26 (2014) 246–258.
- [2] R. Shah, J.D. Gale, M.C. Payne, Comparing the acidities of zeolites and SAPOs from first principles, Chem. Commun. 1 (1997) 131–132.
- [3] M. Yang, D. Fan, Y. Wei, P. Tian, Z. Liu, Recent progress in methanol-to-olefins (MTO) catalysts, Adv. Mater. 31 (2019) 1902181.
- [4] M.Y. Kim, K. Lee, M. Choi, Cooperative effects of secondary mesoporosity and acid site location in Pt/SAPO-11 on n-dodecanehydroisomerization selectivity, J. Catal. 319 (2014) 232–238.
- [5] O.V. Kikhtyanin, A.V. Toktarev, A.B. Ayupov, G.V. Echevsky, Influence of crystallinity on the physico-chemical properties of SAPO-31 and hydroconversion of n-octane over Pt loaded catalysts, Appl. Catal. A-Gen. 378 (2010) 96–106.
- [6] X. Liu, N. Yan, L. Wang, C. Ma, P. Guo, P. Tian, G. Cao, Z. Liu, Landscape of AlPO-based structures and compositions in the database of zeolite structures, Microporous Mesoporous Mater. 280 (2019) 105–115.
- [7] Database of Zeolite Structures. http://www.iza-structure.org/databases/. (Accessed 15 October 2020).
- [8] D. Wang, P. Tian, D. Fan, M. Yang, B. Gao, Y. Qiao, C. Wang, Z. Liu, N-methyldiethanolamine: a multifunctional structure-directing agent for the synthesis of SAPO and AIPO molecular sieves. J, Colloid Interface Sci. 445 (2015) 119–126.
- [9] Z. Han, A.L. Picone, A.M.Z. Slawin, V.R. Seymour, S.E. Ashbrook, W. Zhou, S. P. Thompson, J.E. Parker, P.A. Wright, Novel large-pore aluminophosphatemolecular sieve STA-15 prepared using the tetrapropylammonium cationas a structure directing agent, Chem. Mater. 22 (2010) 338–346.
- [10] S. Seo, T. Yang, J. Shin, D. Jo, X. Zou, S.B. Hong, Two aluminophosphatemolecular sieves built from pairs of enantiomeric structural building units, Angew. Chem. Int. 57 (2018) 3727–3732.
- [11] J. Li, J. Yu, R. Xu, The structure directing and templating effects in the formation of microporous compounds, Chinese J. Inorg. Chem. 20 (2004) 1–16.
- [12] J. Li, A. Corma, J. Yu, Synthesis of new zeolite structures, Chem. Soc. Rev. 44 (2015) 7112–7127.
- [13] M. Moliner, F. Rey, A. Corma, Towards the rational design of efficient organic structure-directing agents for zeolite synthesis, Angew. Chem. Int. 52 (2013) 13880–13889.
- [14] R. Martinez-Franco, M. Moliner, Y. Yun, J. Sun, W. Wan, X. Zou, A. Corma, Synthesis of an extra-large molecular sieve using proton sponges as organic structure-directing agents, Proc. Natl. Acad. Sci. Unit. States Am. 110 (2013) 3749–3754.
- [15] M. Castro, S.J. Warrender, P.A. Wright, D.C. Apperley, Y. Belmabkhout, G. Pirngruber, H.K. Min, M.B. Park, S.B. Hong, Silicoaluminophosphatemolecular sieves STA-7 and STA-14 and their structure-dependent catalytic performance in the conversion of methanol to olefins, J. Phys. Chem. C 113 (2009) 15731–15741.
- [16] M. Castro, R. Garcia, S.J. Warrender, A.M.Z. Slawin, P.A. Wright, P.A. Cox, A. Fecant, C. Mellot-Draznieks, N. Bats, Co-templating and modelling in the rational synthesis of zeolitic solids, Chem. Commun. 33 (2007) 3470–3472.
- [17] G. Majano, K. Raltchev, A. Vicente, S. Mintova, High-yield nanosized (Si) AlPO-41 using ethanol polarity equalization and co-templating synthesis approach, Nanoscale 7 (2015) 5787–5793.
- [18] A. Turrina, R. Carcia, P.A. Cox, J.L. Casci, P.A. Wright, Retrosynthetic cotemplating method for the preparation of silicoaluminophosphate molecular sieves, Chem. Mater. 28 (2016) 4998–5012.
- [19] A. Turrina, R. Garcia, A. E Watts, H.F. Greer, J. Bradley, W. Zhou, P.A. Cox, M. D. Shannon, A. Mayoral, J.L. Casci, P.A. Wright, STA-20: an ABC-6 zeotype structure prepared by co-templating and solved via a hypothetical structure database and STEM-ADF imaging, Chem. Mater. 29 (2017) 2180–2190.
- [20] A. Deneyer, Q. Ke, J. Devos, M. Dusselier, Zeolite synthesis under nonconventional conditions: reagents, reactors, and modi operandi, Chem. Mater. 32 (2020) 4884–4919.
- [21] Q. Huo, R. Xu, S. Li, Z.G. Ma, J.M. Thomas, R.H. Jones, A.M. Chippindale, Synthesis and characterization of a novel extra-large ring of aluminophosphate JDF-20, J. Chem. Soc., Chem. Commun. 12 (1992) 875–876.
- [22] E.R. Cooper, C.D. Andrews, P.S. Wheatley, P.B. Webb, P. Wormald, R.E. Morris, Ionic liquids and eutectic mixtures as solvent and template in synthesis of zeolite analogues, Nature 430 (2004) 1012–1016.
- [23] Y. Wei, Z. Tian, H. Gies, R. Xu, H. Ma, R. Pei, W. Zhang, Y. Xu, L. Wang, K. Li, B. Wang, G. Wen, L. Lin, Ionothermal synthesis of an aluminophosphate molecular sieve with 20-ring pore openings, Angew. Chem. Int. 49 (2010) 5367–5370.

- [24] Y. Lin, L. Zhang, K. Guo, M. Wang, Y. Wei, Co-structure-directing effect in ionothermal synthesis of extra-large-pore aluminophosphate zeotype with -CLO topology, Chem. Eur J. 24 (2018) 2410–2417.
- [25] M. Estermann, L.B. McCusker, C. Baerlocher, A. Merrouche, H. Kessler, Synthstic gallophosphate molecular-sieve with a 2-tetrahedral-atom pore opening, Nature 352 (1991) 320–323.
- [26] J. Su, Y. Wang, J. Lin, J. Liang, J. Sun, X. Zou, A silicogermanate with 20-ring channels directed by a simple quaternary ammonium cation, Dalton Trans. 42 (2013) 1360–1363.
- [27] J. Wen, J. Zhang, J. Jiang, Extra-large pore zeolites: a ten-year updated review, Chem. J. Chinese U. 42 (2021) 101–116.
- [28] D. Fan, P. Tian, S. Xu, Q. Xia, X. Su, L. Zhang, Y. Zhang, Y. He, Z. Liu, A novel solvothermal approach to synthesize SAPO molecular sieves using organic amines as the solvent and template, J. Mater. Chem. 22 (2012) 6568–6574.
- [29] D. Wang, P. Tian, M. Yang, S. Xu, D. Fan, X. Su, Y. Yang, C. Wang, Z. Liu, Synthesis of SAPO-34 with alkanolamines as novel templates and their application for CO₂ separation, Microporous Mesoporous Mater 194 (2014) 8–14, 194.
- [30] D. Fan, P. Tian, X. Su, Y. Yuan, D. Wang, C. Wang, M. Yang, L. Wang, S. Xu, Z. Liu, Aminothermal synthesis of CHA-type SAPO molecular sieves and their catalytic performance in methanol to olefins (MTO) reaction, J. Mater. Chem. A 1 (2013) 14206–14213.
- [31] B. Gao, D. Fan, L. Sun, H. An, F. Fan, S. Xu, P. Tian, Z. Liu, Insights into the aminothermal crystallization process of SAPO-34 and its comparison with hydrothermal system, Microporous Mesoporous Mater. 248 (2017) 204–213.
- [32] M. Afeworki, D.L. Dorset, G.J. Kennedy, K.G. Strohmaier, Synthesis and structure of ECR-40: an ordered SAPO having the MEI framework, in: C. Pts a, E. VanSteen, M. Claeys, L.H. Callanan (Eds.), Recent Advances in the Science and Technology of Zeolites and Related Materials vol. 154, 2004, pp. 1274–1281.
- [33] C. Martineau, B. Bouchevreau, Z. Tian, S.J. Lohmeier, P. Behrens, F. Taulelle, Beyond the limits of X-ray powder diffraction: description of the nonperiodic subnetworks in aluminophosphate-Cloverite by NMR crystallography, Chem. Mater. 23 (2011) 4799–4809.
- [34] D. Li, Y. Xu, Y. Wang, H. Liu, B. Wang, H. Ma, R. Xu, Z. Tian, Ionothermal syntheses and characterizations of cobalt-substituted extra-large pore aluminophosphate molecular sieves with -CLO topology, Microporous Mesoporous Mater. 198 (2014) 153-160.
- [35] M. Afeworki, G. Cao, D.L. Dorset, K.G. Strohmaier, G.J. Kennedy, Multinuclear and multidimensional solid-state NMR characterization of EMM-8, Microporous Mesoporous Mater. 103 (2007) 216–224.
- [36] T. Kodaira, K. Miyazawa, T. Ikeda, Y. Kiyozumi, Synthesis of AlPO4-5 powder by microwave heating: influence of starting gel pH and reaction time, Microporous Mesoporous Mater. 29 (1999) 329–337.
- [37] L. Marchese, A. Frache, E. Gianotti, G. Martra, M. Causa, S. Coluccia, ALPO-34 and SAPO-34 synthesized by using morpholine as templating agent. FTIR and FT-Raman studies of the host-guest and guest-guest interactions within the zeolitic framework, Microporous Mesoporous Mater. 30 (1999) 145–153.
- [38] B. Li, W. Xu, S. Qiu, W. Pang, R. Xu, Quantum-chemical calculation for fluorine ion influence on double four-membered ring of zeolite molecular sieves structure. Chem, J. Chinese U 19 (1998) 930–933.
- [39] N. Yan, L. Wang, X. Liu, P. Wu, T. Sun, S. Xu, J. Han, P. Guo, P. Tian, Z. Liu, A novel approach for facilitating the targeted synthesis of silicoaluminophosphates, J. Mater. Chem. A 6 (2018) 24186–24193.
- [40] J.K. Lee, J.H. Lee, N.H. Ahn, K.H. Choa, S.B. Hong, Solid solution of a zeolite and a framework-bound OSDA-containing molecular sieve, Chem. Sci. 7 (2016) 5805–5814.
- [41] P. Wu, M. Yang, L. Sun, S. Zeng, S. Xu, P. Tian, Z. Liu, Synthesis of nanosized SAPO-34 with the assistance of bifunctional amine and seeds, Chem. Commun. 54 (2018) 11160–11163
- [42] J.K. Lee, J. Shin, N.H. Ahn, A. Turrina, M.B. Park, Y. Byun, S.J. Cho, P.A. Wright, S. B. Hong, Family of molecular sieves containing framework-bound organic structure-directing agents, Angew. Chem. Int. 54 (2015) 11097–11101.
- [43] R.L. Bedard, C.L. Bowes, N. Coombs, A.J. Holmes, T. Jiang, S.J. Kirkby, P. M. Macdonald, A.M. Malek, G.A. Ozin, S. Petrov, N. Plavac, R.A. Ramik, M. R. Steele, D. Young, Cloverite –exploring the 30-angstrom supercage for advanced materials science applications, J. Am. Chem. Soc. 115 (1993) 2300–2313.
- [44] S.L. Lawton, W.J. Rohrbaugh, The framework topology of ZSM-18, a novel zeolite containing rings of 3 (Si, Al)-O species, Science 247 (1990) 1319–1322.
- [45] M.B. Park, S.J. Cho, S.B. Hong, Synthesis of aluminosilicate and gallosilicatezeolites via a charge density mismatch approach and their characterization, J. Am. Chem. Soc. 133 (2011) 1917–1934.
- [46] D. Luo, B. Li, Q. Wang, P. Tian, Z. Liu, Z. Liu, Study on crystallization process of SAPO-5 molecular Sieve. Chem, J. Chinese U 41 (2020) 2442–2448.
- [47] R. Martínez-Franco, Á. Cantín, A. Vidal-Moya, M. Moliner, A. Corma, Selfassembled aromatic molecules as efficient organic structure directing agents to synthesize the silicoaluminophosphate SAPO-42 with isolated Si species, Chem. Mater. 27 (2015) 2981–2989.
- [48] D. Wang, M. Yang, W. Zhang, D. Fan, P. Tian, Z. Liu, Hollow nanocrystals of silicoaluminophosphatemolecular sieves synthesized by an aminothermal cotemplating strategy, CrystEngComm 18 (2016) 1000–1008.